HEFAT2007
5th International Conference on Heat Transfer, Fluid Mechanics and Thermodynamics
Sun City, South Africa
Paper number: CH2

HORIZONTAL TWO-PHASE FLOW CHARACTERISATION AND CLASSIFICATION BASED ON CAPACITANCE MEASUREMENTS

Canière H.*, Bauwens B.§, T'Joen C.*, Willockx A.*, Boullart L.§ and De Paepe M.*

* Department of Flow, Heat and Combustion Mechanics, Ghent University - UGent,
St.-Pietersnieuwstraat 41, Gent, 9000, Belgium
E-mail: Hugo.Caniere@UGent.be

§ Department of Electrical Engineering, Systems and Automation, Ghent University - UGent,
Gebouw Regeltechniek, Technologiepark 913, Zwijnaarde, 9052, Belgium

ABSTRACT

Two-phase flow regime prediction is of great importance for designing evaporators and condensers because the influence of the heat transfer coefficients is strongly related to the flow regimes. These flow regimes are often presented in flow pattern maps. As most flow pattern maps are based on visual observations or transition models fitted to data obtained by visual observations, these maps still lack of objectivity in defining the flow regime transitions. In order to refine the flow regime maps and to add objective flow characteristics to the transitions boundaries, a two-phase flow sensor was developed. The sensor measures the capacitance of the two-phase flow. Because of the difference in dielectric constant of liquid and vapour and the dependency of the capacitance to the internal distribution of liquid and vapour in the cross-section of the tube, the sensor is able to characterize two-phase flow regimes. Measures were taken to improve the accuracy and reliability of the measurements. A charge/discharge transducer with a fast response was built to dynamically measure capacitance differences in the picofarad range. A large number of experiments was done with air-water flow. The setup was able to cover all flow regimes for horizontal flow in a 9mm tube.

The sensor can be used as a flow regime detector. Important for obtaining good classification results, information about vapour-liquid distribution in the cross-section of the tube should be combined with time-dependent information at the measurement location. To obtain both spatial and time information, statistical parameters of the probability density function and the power spectral distributions of the signals were selected to build up a statistical classification model. Decision trees and support vector machines were used for this purpose. A high-speed camera was used as a comparison for the results of the flow detector. More than 90% of the test runs were correctly classified by both statistical techniques.

INTRODUCTION

To reduce energy use by improving coil design, simulation tools for complex circuitry and non-ideal fluid conditions are developed during this decade by Jiang et al. [1] and Bensafi et al. [2], among others. But application specific optimizations made with these kinds of tools are only as good as the models used. Most current heat transfer and pressure drop predictions for two-phase flow are empirical or semi-empirical and lack accuracy, due to the complexity of two-phase flow during flow boiling and flow condensation. This loss of accuracy may be mainly ascribed to the ignorance of the effect of the flow regime when building a correlation from a set of data. Because pressure drop and heat transfer are strongly related to two-phase flow regimes, objective, accurate and reliable flow pattern maps are needed as a strong basis. At present, objective criteria for two-phase flow regime transition are still missing because most models and maps are based on subjective visual observations.

Despite the advances in flow pattern based heat transfer coefficients, there is still a desire for a unified and accurate two phase flow heat transfer model which includes objective flow pattern identification (Thome [3]). Measuring the difference in electrical permittivity of liquid and vapour, useful information about two-phase flows can be obtained. Keska et al. [4] compared four dynamic flow pattern discrimination techniques for multi-phase flow. They found that capacitive measurements have a high potential for flow pattern recognition. Therefore, a capacitance sensor was developed to be able doing online flow regime detection. The sensor signals were studied in the time domain as well as amplitude and frequency domain. A multivariate analysis was done to select useful parameters to build up statistical classification models. Two statistical techniques were used: Decision trees and Support Vector Machines.

CAPACITANCE SENSOR

A concave electrode configuration was chosen because of the possibility to acquire local capacitance measurements with a simple geometry. A scheme of the sensor is shown in Figure 1. The width of the electrodes along the flow direction may not be larger than the local flow characteristics. As smaller electrode width results in lower capacitance, a compromise has to be made. The electrode width was chosen equal to the tube diameter.

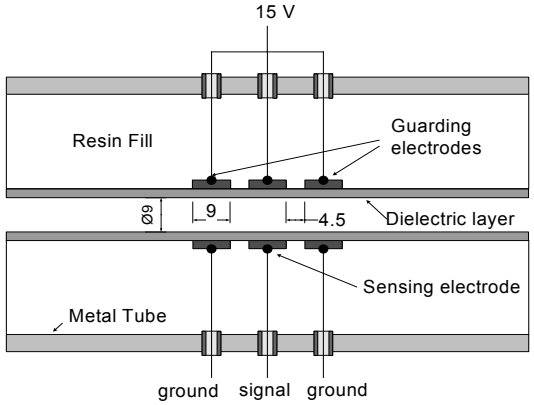

(a) Longitudinal section view

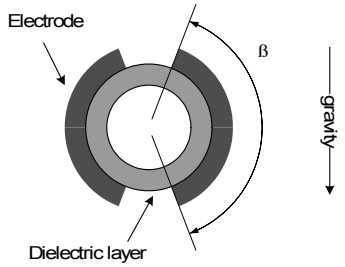

(b) Cross-sectional view

Figure 1 Capacitance sensor scheme

To ensure a proper field line distribution in the direction of the flow, an active guarding technique is used as described by Reinecke and Mewes [5]. Therefore, three pairs of concave electrodes are placed in a row. The middle pair is the sensing pair, the outer pairs are guards. These guards are connected at one end to the source (which is a 15V block signal) and at the other end electrically grounded. The inscribed electrode angle was designed at β=160°. For reasons of mechanical stability, the inner tube with electrodes is placed within an outer metal shielding tube and the space in between was filled with a resin fill. To eliminate influences from the environment, the outer metal tube is grounded as well. For horizontal flow, the electrodes should be positioned one at each side of the tube as shown in Figure 1. This ensured the best flow regime detection for stratified flows.

To measure the capacitance, an electronic circuit is needed to obtain a voltage output for the DAQ system. Measured capacitances are small [pF] and amplification is recommended. The circuit of Yang and Yang [6] was chosen and built for that purpose. It is a four-phase charge/discharge measuring circuit with an adjustable offset, good stray-immunity and high stability. Measurements can be made at 2 frequencies, 1MHz and 100kHz, resulting in two measurement ranges: 0-2pF and 0-20pF. For air-water flow, the 100kHz was chosen. Only the middle electrode is the sensing electrode and is connected to this measurement circuit. The voltage signal was sampled at 1kHz with a National Instruments DAQ system.

SIGNAL ANALYSIS

The sensor was tested for horizontal air-water flow in a small diameter tube of 9mm. Demineralised water was used as test fluid. The temperature was kept constant at 20°C. Flow regimes were determined on the high speed camera visualizations. For classification, three regimes were considered: stratified flow, intermittent flow and annular flow. Stratified flow can have a smooth as well as a wavy interface. Intermittent flow can be slug flow, plug flow, elongated bubble flow etc. All two-phase flows considered as intermittent flow have an irregular or time dependent flow structure and are therefore grouped together.

The most important parameters for heat transfer modeling are dry angle (i.e. the part of the perimeter that is not wetted by liquid) and film thickness or liquid level. By using the three-category classification a distinction can be made between stratified and non-stratified flows as well as a distinction between the ring-shaped annular flows and the more complex flow structures of intermittent flows.

Sensor Signals

In Figure 2, time signals of four flow regimes are plotted. On the ordinate a dimensionless voltage signal, V* (Eq. 1), is shown.

$$V^* = \frac{V_{signal} - V_{air}}{V_{water} - V_{air}} \quad (1)$$

Figure 2(a) shows a stratified flow at near atmospheric pressure (G_{water} = 22.8 kg/m²s and G_{air} = 0.18 kg/m²s). A very slow varying liquid level is clearly visible. In Figure 2(b) the signal of a wavy flow is presented (G_{water} = 43.0 kg/m²s and G_{air} = 18.0 kg/m²s). The liquid level is disturbed by waves due to the interfacial shear stress at high air flow rates. The intermittent flow (G_{water} = 224.5 kg/m²s and G_{air} = 0.57 kg/m²s), shown in Figure 2(c), is a slug flow, characterized by liquid slugs frequently washing the top of the tube. Finally, Figure 4(d) shows an annular flow (G_{water} = 131.8 kg/m²s and G_{air} = 20.8 kg/m²s). This flow regime is characterized by intermediate values of V* with high frequent disturbances.

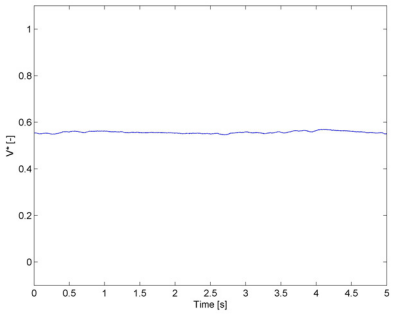

(a) smooth-stratified flow

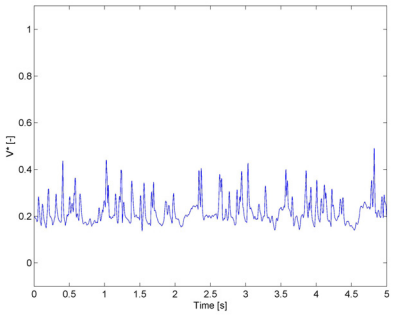

(b) stratified-wavy flow

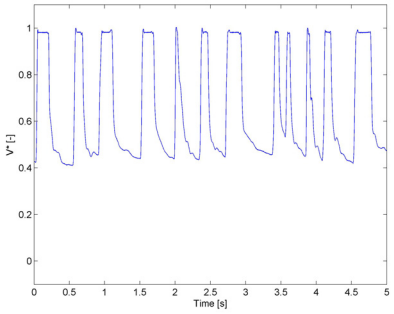

(c) intermittent flow

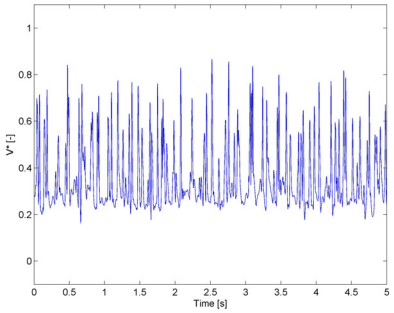

(d) annular flow

Figure 2 Time plots of typical sensor signals

Data-processing

A series of 202 sensor signals was gathered, changing the mass velocities of air and water. Figure 3 shows a flow map of the data points. The mass velocities, G, are plotted on a log-log scale. Transition from intermittent to annular flow is not clearly defined. Data points in that area can be once assigned as annular and another time as intermittent. Visual classification is difficult and inherently subjective, even when based on high speed camera images. Investigating the sensor signals can provide more objectivity.

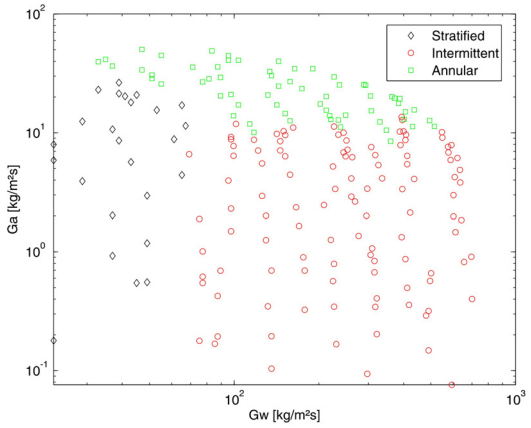

Figure 3 Flow map of experimental data points based on visual classification

From each sensor signal, several statistical parameters were calculated. A first group consists of the statistical moments of the sensor signal, i.e. the average value (M1), the variance (M2), the skewness (M3) and the kurtosis (M4). These parameters determine the shape of the probability density function (PDF) of a signal and represent information of the signal in the amplitude domain. A second group consists of parameters from the frequency domain. Therefore the sensor signal is first transformed using a fast Fourier algorithm and a power spectral distribution (PSD) is calculated. Based on this PSD, the contributions of different bandwidths can be added to define a frequency parameter.

Table 1 shows the number of data points by flow regimes. For statistical modelling reasons of the decision tree technique, this data was divided in a first group of training data and a second independent group of test data. Because intermittent flow covers the largest area on the flow map and the most kinds of sub-regimes, a greater number of test points were selected compared to stratified and annular flow. With the training data the statistical model was built. The model was then evaluated with the independent test data.

Table 1 Number of data points by flow regime

Flow regime	**Training data**	**Test data**	**Total**
Stratified	21	4	25
Intermittent	104	12	114
Annular	57	4	61
Total	**182**	**20**	**202**

For Support Vector Machines, 10-fold cross-validation was performed. This is a slightly different approach. In this case the total dataset of 202 measurement points was randomly divided

in a first group of training data (90% of the total dataset) and a second group of test data (the remaining 10%). Again with the training data the statistical model was built and the independent group of test data used for validation purposes. This training process was then ten times iterated with other random divisions of the data points into the training and test group. Finally the average accuracy was calculated.

Multi-variate analysis

The statistical parameters of the data points were investigated for their ability of flow regime identification. The average value (AVG) and the variance (M2) of the signal amplitude together with a high frequency contribution factor (HFCF) were found to be most suitable for this purpose. The HFCF is basically the addition of the power spectra contribution, based on a Fourier transform, starting from 10Hz up to 100Hz. On Figure 4 a multivariate plot of these three parameters is presented. Each subplot in the matrix is a scatter plot of the variables at the row and column index. On the diagonal of the plot matrix, a histogram of the respective variable is shown.

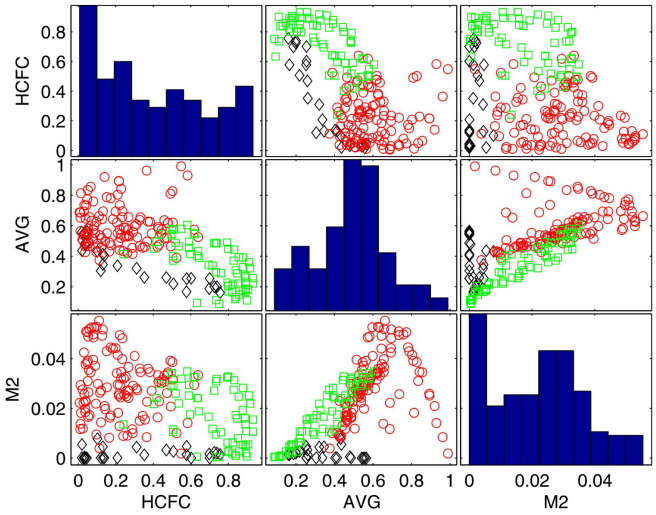

Figure 4 Multivariate analysis of the sensor signals (◊ = stratified – o = intermittent – □ = annular)

Annular flows typically have a high HFCF and low to intermediate values of AVG and M2. Stratified flows have low to intermediate values of AVG, but only low values of M2. The HFCF is spread over the full range because both smooth and wavy stratified flows are present. Intermittent flows have intermediate to high values of AVG and M2 and low to intermediate values of HFCF. Figure 4 clearly shows the ability of the sensor signals for flow pattern classification by combining amplitude information (AVG, M2) and frequency information (HFCF) in a non-linear way. A single parameter will not be sufficient. These variables are now used to build a statistical model for two-phase flow classification. The wide transition area between annular and intermittent flow is still present in the multivariate plots. This will limit the accuracy of the model.

STATISTICAL CLASSIFICATION METHODS

Decision trees

Decision trees are a simple and successful technique for classification learning [7]. An object represented by continuously distributed features x_i, i = 1..n is classified according to a sequence of questions. Traditionally these questions are x_j > th, with th a splitting value. Every nod represents a question and every leaf gives a classification result, denoted as 1...k. The tree is grown using the Gini index, an index that measures the diversity in a set of samples:

$$g(S) = 1 - \sum_{i=1}^{k} p_i^2 \qquad (2)$$

p_i, i=1...k is the fraction of elements from class i to the total number of elements in the dataset S. The Gini index for a decision, dec = xi < th, that divides the dataset S in the two datasets S_1 and S_2 is:

$$g(i,th) = g(S_1) + g(S_2) - g(S) \qquad (3)$$

S_1 is the subset of data that fulfil the condition of the question, S_2 the complementary subset. The traditional training algorithm is an iterative growing algorithm:

1. Associate the full dataset to a first node. This node is the root of the tree.
2. While all leaves which have an associated set of more than 10 elements from different classes: choose such a leaf with associated set S.
   - Calculate for every feature: i = 1...n and for every possible splitting value th the Gini index g(i, th) on S.
   - Replace the leaf by a new node that represents the decision with the highest Gini-index. Associate the corresponding subsets of S to the 2 new leaves.

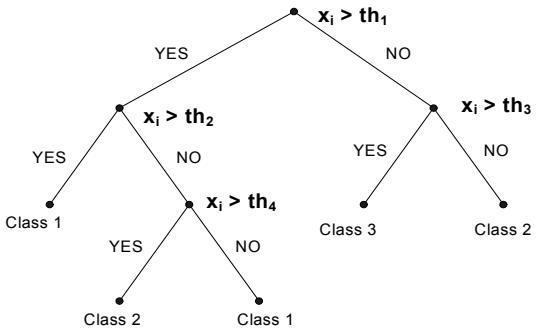

Figure 5 Illustration of a decision tree

In Figure 5, an illustration of a decision tree is shown. Applying this statistical technique to a dataset of sensor signals, AVG, M2 and HFCF were selected as features x_i. First, consider the full dataset. Calculate the Gini-index with Eq. (3) for every value of th and every feature. Select the question with the highest Gini-index and divide the dataset S into the subsets S_1 and S_2. Two leaves are grown. Repeat the same procedure for every leaf that has a subset of more than 10 elements and

for which the elements does not belong to the same flow regime.

Table 2 shows the results of two decision trees trained and tested with the sensor data. Tree 1 was trained using the AVG and the HFCF of the signals, training of Tree 2 was performed using the AVG, M2 and HFCF. # Nodes is the number of leaves of the tree. The resubstitution cost is obtained by evaluating the training data and counting the number of mismatches. The cross cost is a 10-fold cross-validation only based on the training data of Table 1. Mismatch is the number of misclassifications of the second group of independent test data. Finally Test Cost is the sum over all terminal nodes of the estimated probability of that node times the number of misclassifications.

With a tree that has many branches, there is a danger that it fits the training data set well but would not do a good job at predicting new values. Some of its lower branches might be strongly affected by outliers and other artefacts of the current data set. A simpler tree that avoids this problem of overfitting can be preferable. Therefore decision trees have to be pruned in a way that the size of the tree decreases but the cost of the performance of the tree does not augment to much. Pruning is performed by comparing the performance increase of an extra splitting of a branch to the amount of leaves of the branch. The cross-validation cost was used as performance indicator. The best tree is the one that has a cost that is no more than one standard error above the minimum value along the cross-validation line. The decision trees obtained with the optimization procedure are labelled as 1b and 2b and their results are also shown in Table 2.

Table 2 Results of decision trees

Tree	1a	1b	2a	2b
# Nodes	15	7	13	3
Resub. cost	4.95%	8.79%	1.65%	10.4%
Cross cost	18.1%	14.2%	14.3%	12.6%
Mismatch	1/20	0/20	0/20	2/20
Test Cost	0%	8.6%	0%	8.6%

As expected, the results of Tree 2 are better than the results of Tree 1 and the resubstitution cost augments when the pruned trees are evaluated. Very high accuracies were found for both decision trees and misclassification only occurs at the ambiguous transition zone between annular and intermittent flow.

Support vector machines

Support vector machines (SVM) are another popular approach to the problem of classification. The construction of the SVM algorithm is based on an elaborate statistical framework which prevents the algorithm for overfitting. In many cases the performance of SVM was shown to be comparable with that of neural networks [8-9].

Any solution for a classification algorithm is represented by a decision rule which decides in what class a given signal will be classified. During the training stage, the decision rule is looked for which best fits the set of training data: $(\mathbf{x}_1, y_1), (\mathbf{x}_2, y_2), \ldots, (\mathbf{x}_n, y_n)$. $\mathbf{x}_i$ is a vector representing the features of each data point and y_i represents the class of the data point. The sensor features selected from the multivariate analyses were used as training data: AVG, M2 and HFCF as input variables $\mathbf{x}_i$ and the visual classifications based on the high-speed camera images as training output y_i. A *cost* value can be calculated for every decision rule. This cost value is used to find the optimal decision rule.

.

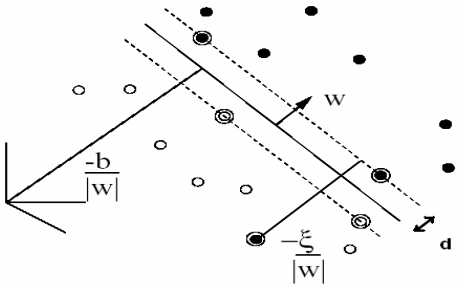

Figure 5 Example of a linear Support Vector Machine with non-separable data (Burges [10])

Figure 5 illustrates the decision rule used in a linear Support Vector Machine with non-separable data. Two classes are considered: dots and circles. The decision rule is represented by a line in the plane. When using this decision rule, every sample above the line will be classified by the SVM as a dot, all other samples as circles. The rule in this example makes one mistake, because there is a dot below the line. To measure the quality of this decision rule, two borders are drawn (dotted lines in Figure 5), one above and another below the full line, on an equal distance d. For every 'dot' below the upper border, the orthogonal distance is measured to this border $\xi_i(d)$. For every 'circle' above the lower border, the distance $\xi'_i(d)$ is measured to this lower border. The cost of the decision rule is then defined by:

$$Min\left\{\frac{1}{d} + C_1 \sum_{i:y_i='dot'} \xi_i(d) + C_2 \sum_{i:y_i='circle'} \xi'_i(d)\right\} \quad (4)$$

for all values of d. C_1 and C_2 are weight parameters that need to be chosen. Normally C_1 is set equal to C_2. This means that misclassification is equally important for both classes, when both classes contain the same amount of data points. However, the data set created by the sensor was strongly unbalanced. The intermittent flow class has a lot more data points than the stratified flow class or the annular flow class. This results in a higher contribution to the cost value from the data set with the highest number of data points, because it is more probable that the number of misclassifications in that class will be higher. For that, $C_1 n_1 = C_2 n_2 = C$ was used with n_1 and n_2 the number of data points in each class. The decision rule is now [11]:

$$F(\mathbf{x}) = \mathbf{w} \cdot \mathbf{x} + b \quad \text{with} \quad \mathbf{w} = \sum_{i=1}^{n} \alpha_i \mathbf{x}_i \quad (5)$$

with i the dimensional index. This **w** determines the normal direction of the decision rule line and b the position. In the training stage the coefficients α_i and b are searched for to

minimize Eq. (2). The sign of F(**x**) determines whether the data point **x** is situated above or below the decision line.

In order to represent a non-linear decision rule, the same analysis is performed after mapping the data vectors $\mathbf{x}_1$,... $\mathbf{x}_n$ into a high dimensional space into the vectors $\boldsymbol{\varphi}(\mathbf{x}_1)$,..., $\boldsymbol{\varphi}(\mathbf{x}_n)$. To evaluate Eq. (4) and Eq. (5), only the function $K(\mathbf{x},\mathbf{x}') = \boldsymbol{\varphi}(\mathbf{x})\cdot\boldsymbol{\varphi}(\mathbf{x}')$ expressing the dot-product in the high dimensional space is necessary, not the explicit mapping $\boldsymbol{\varphi}$. As in the standard case, this dot product is chosen to be the radial basis function [11]:

$$K(\mathbf{x},\mathbf{x}') = \exp\left(\frac{-\sum_i (x^i - x'^i)^2}{2\sigma^2}\right) \quad (6)$$

with i the dimensional index and σ another parameter that needs to be chosen. The decision rule is determined by the sign of F(**x**), Eq. (5)

$$F(\mathbf{x}) = \sum_{i=1}^{n} \alpha_i K(\mathbf{x}_i, \mathbf{x}) + \mathrm{b} \quad (7)$$

again, α_i and b are learned during the training stage. This form of the decision rule is the same as for a radial basis neural network. For every couple of tuning parameters (σ,C) a unique classification solution is found. These parameters are tuned by a grid search to find the optimum model accuracy. This means that a rectangular grid of (σ,C)-couples is created. For every couple, the model is evaluated by the number of misclassifications using a 10-fold cross-validation. A second, finer grid is then evaluated near the maximum value, to find the optimum (σ,C)-couple.

An SVM was trained and tested using the AVG, M2 and HFCF of the sensor signals. The libsvm software was used to perform the analyses [12]. An overall 10-fold cross-validation accuracy of 92.1% was found with the sensor signal data. The accuracy for data samples from the stratified flow, intermittent and annular flow was 100%, 90.3% and 92.1% respectively. Misclassification only occurs at the transition zones between neighboring flow regimes, especially the broad zone between annular and intermittent flow. This proofs the ability of the sensor for online flow regime detection.

CONCLUSIONS

For the purpose of objective flow pattern identification, a capacitance sensor was developed for horizontal two-phase flow in small diameter tubes. A large series of experiments was done with horizontal air-water flow in a 9mm tube. Classification was made visually based on high speed camera images.

A multivariate analysis of statistical parameters of the signals shows the possibility of two-phase flow classification by combining in a non-linear way, the average and variance of the signal amplitude together with a high frequency contribution factor, i.e. combining spatial and time dependent information.

Two statistical techniques were use for building a classification model, based on these sensor parameters. Decision trees and support vector machines. Comparable accuracies were found for both techniques. Cross-accuracies of 90% and higher were obtained with the experimental data. Misclassification was mainly due to the wide and ambiguous transition zone between annular and intermittent flow.

ACKNOWLEDGMENTS

The authors would like to express gratitude to the BOF fund (B/06634) of the Ghent University - UGent which provided support for this study and thank Robert Gillis and Patrick De Pue for their technical experience and help.

REFERENCES

[1] Jiang H.B., Aute V. and Radermacher R., Coildesigner: A General-Purpose Simulation and Design Tool for Air-to-Refrigerant Heat Exchangers, *International Journal of Refrigeration*, Vol. 29, 2006, pp. 601-10.

[2] Bensafi A., Borg S. and Parent D., Cyrano: A Computational Model for the Detailed Design of Plate-Fin-and-Tube Heat Exchangers Using Pure and Mixed Refrigerants, *International Journal of Refrigeration,* Vol. 20, 1997, pp. 218-28.

[3] Thome J.R., Two-Phase Heat Transfer Using No-Phase Flow Models? *Heat Transfer Engineering,* Vol. 25, 2004, pp. 1-2.

[4] Keska J.K., Smith M.D. and Williams B.E., Comparison Study of a Cluster of Four Dynamic Flow Pattern Discrimination Techniques for Multi-Phase Flow, *Flow Measurement and Instrumentation,* Vol. 10, 1999, pp. 65-77.

[5] Reinecke N. and Mewes D., Multielectrode Capacitance Sensors for the Visualization of Transient Two-Phase Flows, *Experimental Thermal and Fluid Science,* Vol. 15, 1997, pp. 253-66.

[6] Yang S.X. and Yang W.Q., A Portable Stray-Immune Capacitance Meter, *Review of Scientific Instruments,* Vol. 73, 2002, pp. 1958-61.

[7] Breiman L., Friedman J.H., Olshen R.A. and Stone C.J., Classification and Regression Trees*,* 1984*,* CRC Press, Baca Raton, Florida, USA.

[8] Schölkopf B. and Smola A., Learning with Kernels: Support Vector Machines, Regularization, Optimization, and Beyond, 2002, MIT Press, Cambridge, MA, USA.

[8] Huang Z., Chen H., Hsu C.J., Chen W.H. and Wu S.S., Credit rating analysis with support vector machines and neural networks: a market comparative study, *Decision Support Systems,* Vol. 37, 2004, pp. 543-558.

[9] Van Looy S., Vander Cruyssen B., Meeus J., Wyns B., Westhovens R., Durez P., Van den Bosch F., Vastesaeger N., Geldhof A., Boullart L. and De Keyser F., Prediction of dose escalation for rheumatoid arthritis patients under infliximab treatment, *Engineering Applications of Artificial Intelligence,* Vol. 19, 2006, pp. 819-828.

[10] Burges C.J.C., A Tutorial on Support Vector Machines for Pattern Recognition, *Data Mining and Knowledge Discovery,* Vol. 2, 1998, pp. 121-167.

[11] Schölkopf B. and Smola A., Learning with Kernels: Support Vector Machines, Regularization, Optimization, and Beyond, MIT Press, Cambridge, MA, USA, 2002.

[12]Chang C.C. and Lin C.J., LIBSVM: a library for support vector machines, 2001. Software available at: http://www.csie.ntu.edu.tw/~cjlin/libsvm.